Ann. Geophys., 26, 2043–2052, 2008
www.ann-geophys.net/26/2043/2008/

Annales Geophysicae

Analysis of relationships between ultraviolet radiation (295–385 nm) and aerosols as well as shortwave radiation in North China Plain

X. Xia[1], **Z. Li**[2], **P. Wang**[1], **M. Cribb**[2], **H. Chen**[1], **and Y. Zhao**[3]

[1]LAGEO, Institute of Atmospheric Physics, Chinese Academy of Sciences, Beijing, China
[2]Department of Atmospheric and Oceanic Science and ESSIC, University of Maryland, MD, USA
[3]Chinese Academy of Meteorological Sciences, Chinese Meteorological Administration, Beijing, China

Received: 19 November 2007 – Revised: 26 June 2008 – Accepted: 17 July 2008 – Published: 28 July 2008

Abstract. The fraction of ultraviolet (UV) radiation to broadband shortwave (SW) radiation (F_{UV}=UV/SW) and the influences of aerosol, precipitable water vapor content (PWV) and snow on F_{UV} were examined using two year's worth of ground-based measurements of relevant variables in northern China. The annual mean F_{UV} was 3.85%. Larger monthly values occurred in summer and minimum appeared in winter. Under cloudless condition, F_{UV} decreased linearly with $\tau_{500\,nm}$ and the resulting regression indicated a reduction of about 26% in daily F_{UV} per unit $\tau_{500\,nm}$, implying that aerosol is an efficient agent in lowering the ground-level UV radiation, especially when the sun is high. Given that the annual mean $\tau_{500\,nm}$ is 0.82, aerosol induced reduction in surface UV radiation was from 24% to 74% when the solar zenith angle (θ) changed from 20° to 80°. One cm of PWV led to an increase of about 17% in daily F_{UV}. One case study of snow influence on surface irradiance showed that UV and SW radiation increased simultaneously when the ground was covered with snow, but SW radiation increased much less than UV radiation. Accordingly, F_{UV} increased by 20% for this case. Models were developed to describe the dependence of instantaneous UV radiation on aerosol optical depth, the cosine of the solar zenith angle (μ), and clearness index (Kt) under both clear and all-weather conditions.

Keywords. Atmospheric composition and structure (Aerosols and particles) – Meteorology and atmospheric dynamics (Radiative processes; General or miscellaneous)

Correspondence to: X. Xia
(xiaxiangao2000@yahoo.com)

1 Introduction

Ultraviolet (UV) radiation, defined as electromagnetic radiation having wavelengths within the range 100–400 nm, composes 8.73% of the solar spectrum at the top of the atmosphere and represents a smaller part of the spectrum at the Earth's surface (Foyo-Moreno et al., 1998; Cañada et al., 2000; Ogunjobi and Kim, 2004). However, UV radiation is very important because of its biological and photochemical effects, therefore, understanding the amount of UV near the Earth's surface and its spatial and temporal availability is of significance to a wide range of disciplines, for example, forestry, agriculture and oceanography (Zerefos, 1997; He et al., 2002), as well as air pollution and human health (Diffey, 1991; Lü et al., 1997). Major atmospheric constituents influencing surface UV radiation variability include cloudiness, aerosols and ozone (Wang et al., 1999; Calbó et al., 2005). The albedo of a snow-free surface in the UV range is generally within 1–5%, but if covered by snow, the albedo may be up to 60 and 95%. As such, multiple reflections between the ground surface and the atmosphere can dramatically increase surface UV radiation (Renaud et al., 2000). The relative effect of these factors depends on the time scale and UV bands. For example, it was affirmed that the main UV day-to-day variability was induced by cloudiness and aerosols but not by ozone (Krzyscin and Puchalski, 1998; Papayannis et al., 1998). Aerosols attenuate more UV irradiance than ozone does under cloudless conditions for wavelengths longer than 315 nm (Koronakis et al., 2002; Kalashnikova et al., 2007). Our understanding of UV radiative transfer in the atmosphere, spatial-temporal variations and influential factors (aerosol, cloud, snow cover, etc.) have improved substantially thanks to advances in radiative transfer modeling, ground-based and space-borne observation techniques and remote sensing (Wang et al., 1999; Li et al., 2000; Petteri

Published by Copernicus Publications on behalf of the European Geosciences Union.

et al., 2000; Ciren and Li, 2003; Foyo-Moreno et al., 2003; Renaud et al., 2000; Schwander et al., 2002; Calbó et al., 2005).

Given the fundamental role that UV radiation plays and the lack of long-term measurements, two methods were widely used for the determination of UV radiation from ground-based measurements. One is to use radiative transfer models and the other is to develop empirical models based on parameters usually measured at most of the radiometric stations. If the parameters are available at numerous locations over long periods, the geographical distribution of UV and the long-term trend can be determined (Boderker and McKenzie, 1996). UV radiation has been measured or computed from such commonly available variables, such as the solar zenith angle (θ) and the clearness index (*Kt)*, where *Kt* is defined as the ratio of shortwave (SW) to extraterrestrial irradiance on a horizontal surface. Some empirical equations have been developed to estimate UV from SW (Foyo-Moreno et al., 1999; Cañada et al., 2000; Ogunjobi and Kim, 2004). The Artificial Neural Network has also been used to model the UV from SW (Alados et al., 2004, 2007; Barbero et al., 2006). Surface UV can be retrieved from satellite UV measurement (Krotokov et al., 1998; Li et al., 2000; Ciren and Li, 2003), which allows characterizing the spatial and temporal variability of UV radiation.

The first objective of this study is to understand the influence of the atmosphere and the surface on the UV ratio to SW. The second is to establish a clear-sky model and an all-weather empirical model. The paper is organized as follows. A brief introduction to the site, instrument and observations is presented in the following section. Section 3 discusses the impacts of aerosol, precipitable water vapor content (PWV) and snow-covered ground on UV radiation. The two empirical models are described in the following two sections. A summary is provided in Sect. 6.

2 Site, instrument and measurements

A project entitled the "East Asian Study of Tropospheric Aerosols: an International Regional Experiment" (EAST-AIRE) commenced in 2004 aimed to gain insight about aerosol properties and their climatic and environmental effects in China (Li et al., 2007a). An important goal of the project is to establish several super-sites in China to measure aerosol, cloud and radiative quantities on a long-term basis. In September 2004, the first super-site was established at Xianghe (39.753° N, 116.961° E, 30 m above sea level), where a set of solar radiometers was installed side by side on the roof a four-story building where the field of view is unobstructed in all directions (Xia et al., 2007a). More than two year's worth of continuous measurements of SW and UV irradiance ($\mathrm{W\,m^{-2}}$) has been made. Measurements from October 2004 to September 2006 were used in the analysis.

The radiometers used to measure global SW radiation were Kipp Zonen CM21 and CM11. In addition, direct and diffuse radiations are measured by an Eppley normal incidence pyrheliometer and a black and white radiometer, both mounted on an EKO STR-22 solar tracker. Global SW radiation is thus measured with four instruments that provide independent measurements for inter-comparison and validation purposes. This turns out to be a very effective means of quality control. The global UV radiation on a horizontal surface is measured by an Eppley TUVR radiometer. The instrument utilizes a hermetically sealed selenium barrier-layer cell that is protected by a quartz window. An encapsulated narrow band-pass filter limits the spectral response of the photocell to the wavelength interval 295 to 385 nm. The cosine error of the instrument is better than $\pm 3.5\%$ for θ range 0°–75°, with temperature dependence 0.3% per degree over ambient temperature range $-10°$ to 40° and the linearity is within 2% from 0 to $70\,\mathrm{W\,m^{-2}}$ (http://www.eppleylab.com/; Foyo-Moreno et al., 1999). We limited our analysis to θ less than 85°, in order to minimize the cosine error. Daily checks were made to ensure that the radiometers were positioned horizontally and that the domes of radiometers were clean. Instrument sensitivity degradation was monitored via annual comparisons against new or newly calibrated radiometers that were brought to China for establishing new observation sites. The sensitivities of CM21 and TUVR were estimated to decrease by about 1% and 2% per year, respectively. The measurement uncertainty of global SW is less than 3% (Long and Ackerman, 2000). The relative error of the TUVR radiometer is estimated to be less than 10% (Grimnes et al., 2002), but as pointed out by Foyo-Moreno et al. (1998), the value can be as high as 15%. Daily and hourly means are computed from 1-min raw data. Aerosol optical depths (τ) at seven wavelengths are retrieved from direct spectral solar radiation measurements made by a CIMEL Sun photometer (CE-318). The measurements at 940 nm are used to retrieve PWV content (cm) (Holben et al., 1998). Level 2 data (cloud-screened and quality controlled) are obtained from the Aerosol Robotic Network (AERONET) data pool. Aerosol optical properties and its radiative effects are studied using a combination of aerosol and surface radiation data (Li et al., 2007b; Xia et al., 2007a).

3 UV fraction and its dependence on PWV, aerosol and snow

The monthly UV fractions (expressed as percentage) and the standard deviations are presented in Table 1. Minimum monthly values of F_{UV} appeared in winter (DJF) and maximum monthly values occurred in summer (JJA). F_{UV} in spring (MAM) was in the middle and was close to that in autumn (SON). The fact that relatively higher values of F_{UV} occurred in summer was partly due to higher PWV content in this season. In more humid conditions, the absorption

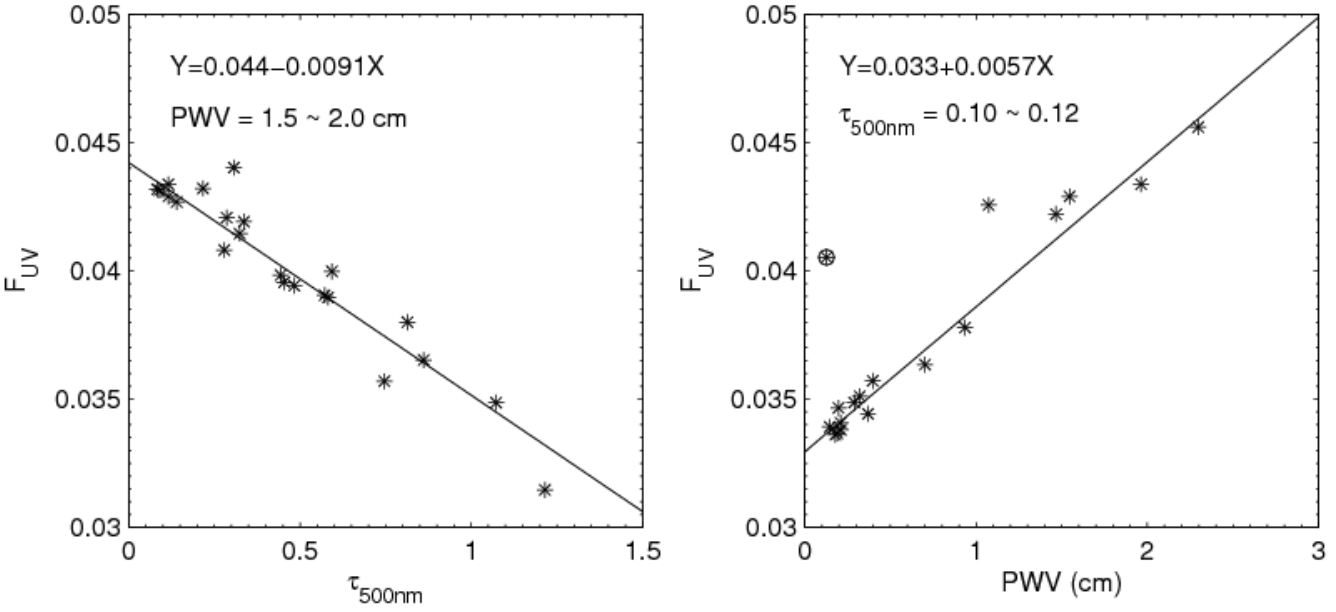

Fig. 1. The dependence of the fraction of UV to solar radiation (F_{UV}) on aerosol optical depth at 500 nm ($\tau_{500\,nm}$) for daily precipitable water vapor content (PWV) of 1.5∼2.0 cm (left) and on PWV for daily $\tau_{500\,nm}$ of 0.10∼0.12 (right).

Table 1. Monthly mean fraction of UV to solar radiation and standard deviation (presented as percentage).

Mon	Jan	Feb	Mar	Apr	May	Jun	Jul	Aug	Sep	Oct	Nov	Dec
F_{UV}	3.42	3.70	3.67	3.73	4.04	3.88	4.44	4.37	4.17	3.78	3.53	3.52
STD	0.44	0.49	0.30	0.41	0.54	0.56	0.58	0.62	0.53	0.54	0.54	0.40

of solar radiation in the infrared region of the solar spectrum is enhanced, whereas absorption in the UV region does not vary significantly. Thus, an increase in F_{UV} under humid conditions and a decrease under dry conditions skies is expected. The annual mean F_{UV} is about 3.85%. In the Mediterranean area, UV percentage ranged from 3.7% to 4.9% (Foyo-Moreno et al., 1999; Koronakis et al., 2002; Cañada et al., 2000, 2003). Relatively lower F_{UV} in northern China is partly due to heavy aerosol loading. The attenuation of UV by aerosols is generally considerably larger than that in the whole SW range because aerosol extinction generally decreases with wavelength. To quantitatively examine the substantial reduction in F_{UV} induced by aerosols and the remarkable increase in F_{UV} due to PWV, the effects of aerosol and PWV on F_{UV} were quantified for clear-sky days with PWV ranging from 1.5 to 2.0 cm and low aerosol days ($0.1<\tau_{500\,nm}<0.12$), respectively (see Fig. 1). Discrimination of clear sky is achieved using an empirical clear-sky detection algorithm proposed by Long and Ackerman (2000), with some modifications to better cope with the specific conditions under study (Xia et al., 2007a). As seen from Fig. 1, F_{UV} decreased linearly with $\tau_{500\,nm}$ and the resulting regression indicated a reduction of about 26% in daily F_{UV} per one unit increase in $\tau_{500\,nm}$. With regard to the PWV effect, one cm increase in PWV led to an increase of about 17% in daily F_{UV}. Note that there is an outlier represented by a solid circle in the left panel of Fig. 1. PWV is about 0.12 but daily F_{UV} is above 0.041, larger than the expectation by about 20%. It occurred on 8 February 2006, a clear and clean day when $\tau_{500\,nm}$ was 0.097 but the surface was covered by snow. Aerosol loading and PWV on 2 February 2005 are very close to those on 8 February 2006 but the surface is snow free. Measurements of direct, diffuse, global SW, UV and UV fraction for these two days are shown in Fig. 2. Difference in direct radiations was negligible, especially when μ is within 0.35∼0.45 (Fig. 2a), however, diffuse and UV radiation increased by 38% and 30% on 8 February 2006, due to increased multiple reflections between the snow-covered surface and the atmosphere. SW increased by 8% (Fig. 2c) which is much less than UV; as a result, the UV fraction increased by 20% (Fig. 2e). It should be noted that only one snow-covered case has been studied here, so assessment of snow influence on UV radiation needs further study.

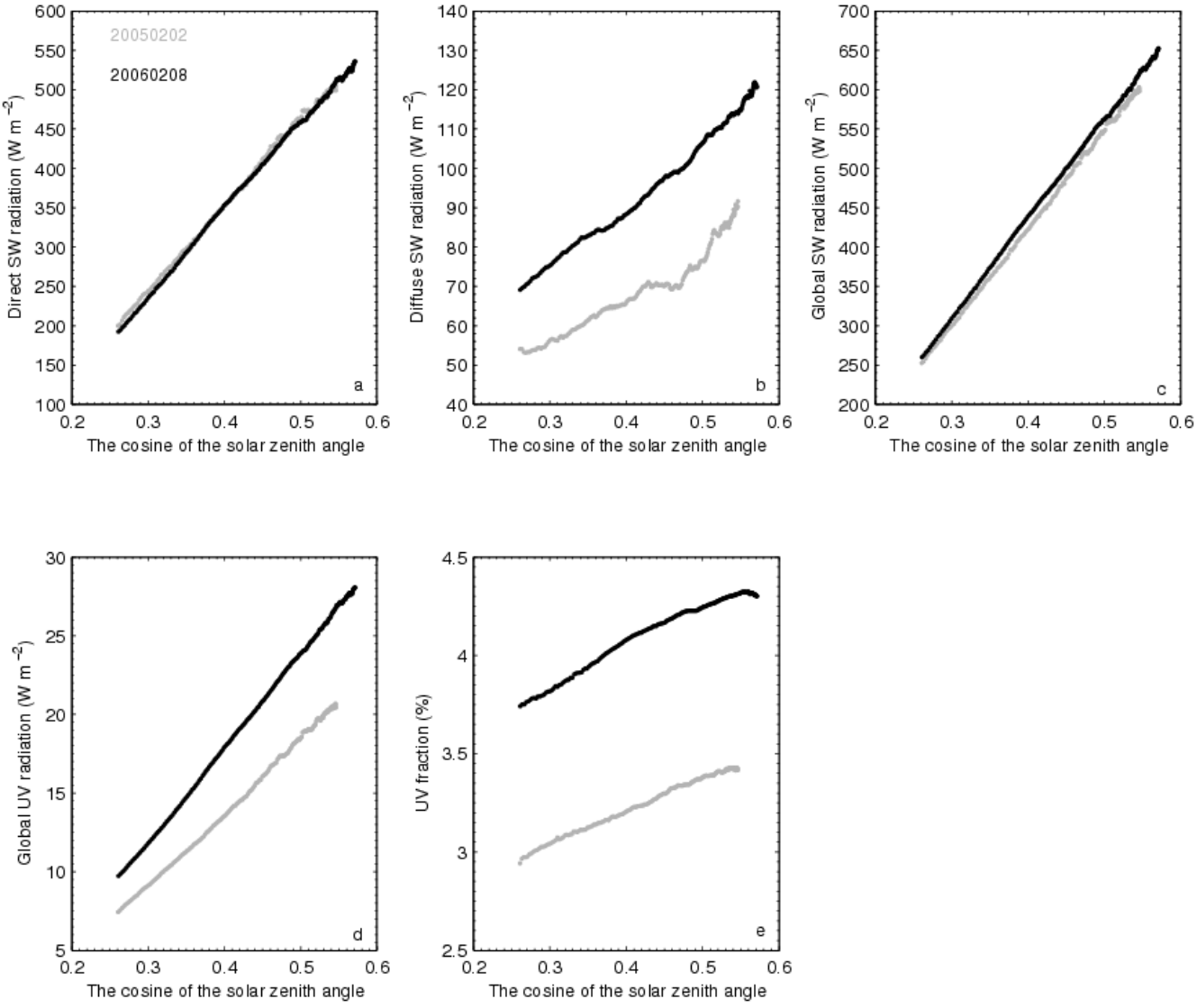

Fig. 2. Comparison of direct, diffuse, global SW, UV radiation and UV fraction between two days: 2 February 2005 and 8 February 2006. The attenuation of solar radiation is nearly identical but the ground is snow covered on 8 February 2006 and not on 2 February 2005.

4 A clear-sky model of UV radiation

In order to develop an empirical model concerning aerosol effects on surface UV radiation, data were first divided into two groups: one group for model development, comprised of 75% of all the data (randomly chosen), and another group for validation, comprised of the remainder of the data. The instantaneous aerosol attenuation of UV radiation depends heavily on θ. In order to remove this dependence so that the aerosol effects on surface UV radiation can be isolated, the relationships between aerosols and UV radiation were analyzed separately for narrow ranges of θ. Scatter plots of measured surface UV radiation as a function of $\tau_{500\,\mathrm{nm}}$ for nine ranges of θ are shown in Fig. 3. The resulting regression analysis showed that about 90% of the variance in UV was explained by $\tau_{500\,\mathrm{nm}}$. The overall effect of aerosols is to induce a notable reduction in surface UV radiation. The dependence of UV on $\tau_{500\,\mathrm{nm}}$ can be described using the following equation.

$$\mathrm{UV} = P_1 \times e^{P_2 \times \tau_{500\,\mathrm{nm}}} + P_3, \quad (1)$$

where P_1 (W m^{-2}), P_2 and P_3 (W m^{-2}) can be derived from the least-squares fitting of UV and $\tau_{500\,\mathrm{nm}}$ for narrow ranges of θ (see Table 2). They are then parameterized as the functions of the cosine of the solar zenith angle (μ), as shown in Fig. 4, i.e. $P_1 = a_1 + a_2 \times \mu$; $P_2 = a_3 + a_4 \times \mu$; $P_3 = a_5 \times \mu^{a_6}$, where a_i (i=1∼6) are derived from the least-squares fitting of data. Variances in P_1, P_3 are explained by 83% and 78%.

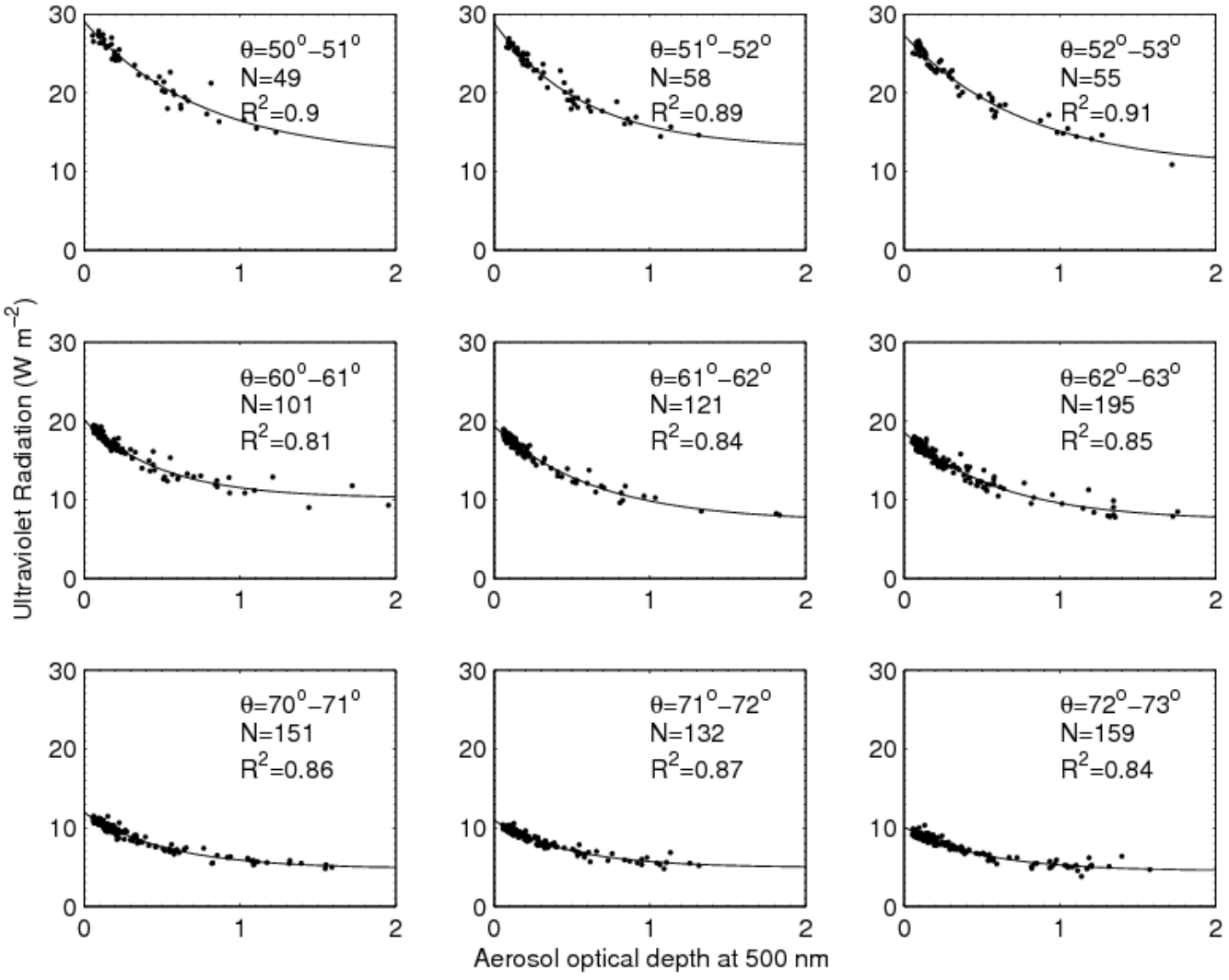

Fig. 3. The dependence of UV radiation on aerosol optical depth at 500 nm for nine solar zenith angles. The line represents the fitting results of the data using an exponential equation.

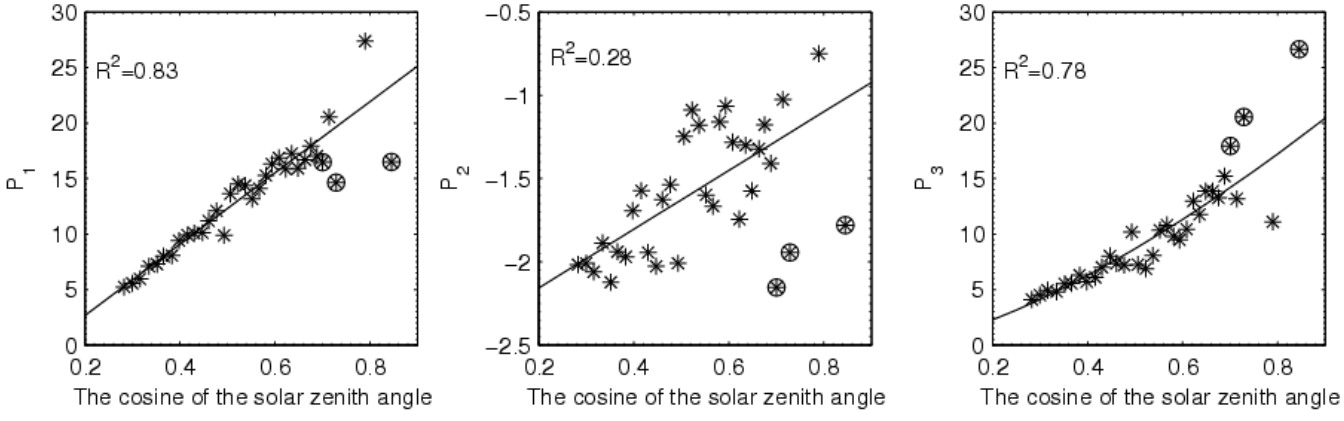

Fig. 4. Scatter plots of the parameters of the exponential equation as a function of the cosine of the solar zenith angle. The black lines represent the fitting results using a linear equation (left, middle) and a power-law equation (right).

Table 2. The parameters of Eq. (1): P_1 (W m^{-2}), P_2 and P_3 (W m^{-2}) derived from the least-squares fitting of UV and $\tau_{500\,\mathrm{nm}}$ for narrow ranges of solar zenith angle. R^2 represents the coefficient of determination.

μ	0.85	0.79	0.76	0.73	0.71	0.70	0.69	0.68	0.66
P_1	16.51	27.38	38.87	14.63	20.55	16.48	17.04	17.94	16.70
P_2	−1.78	−0.75	−0.53	−1.94	−1.03	−2.15	−1.41	−1.18	−1.32
P_3	26.65	11.10	−2.55	20.54	13.18	17.93	15.21	13.26	13.87
R^2	0.83	0.84	0.91	0.79	0.88	0.86	0.87	0.92	0.86
μ	0.65	0.64	0.62	0.61	0.59	0.58	0.57	0.55	0.54
P_1	15.93	17.25	15.85	16.86	16.31	15.29	14.10	13.19	14.37
P_2	−1.57	−1.30	−1.74	−1.28	−1.07	−1.16	−1.67	−1.60	−1.18
P_3	13.86	11.77	12.96	10.43	9.48	9.80	10.80	10.35	8.07
R^2	0.89	0.90	0.89	0.91	0.90	0.91	0.93	0.91	0.93
μ	0.52	0.51	0.49	0.48	0.46	0.45	0.43	0.42	0.40
P_1	14.50	13.63	9.89	12.08	11.18	10.11	10.08	9.91	9.41
P_2	−1.09	−1.25	−2.01	−1.54	−1.63	−2.03	−1.94	−1.57	−1.69
P_3	6.88	7.25	10.17	7.21	7.35	8.03	7.02	6.10	5.70
R^2	0.95	0.86	0.81	0.84	0.85	0.84	0.89	0.84	0.84
μ	0.38	0.37	0.35	0.33	0.32	0.30	0.28	0.27	
P_1	8.07	8.01	7.28	7.09	5.96	5.57	5.24	4.82	
P_2	−1.97	−1.94	−2.12	−1.89	−2.06	−2.01	−2.02	−2.29	
P_3	6.30	5.56	5.54	4.80	4.93	4.51	4.10	4.04	
R^2	0.83	0.87	0.83	0.86	0.87	0.84	0.86	0.87	

The variance in P_2 explained by μ is only 28% partly due to the influence from three outliers (circles in Fig. 4). If these three points are excluded in the analysis, the variance of P_2 explained by μ rises to 70%, so this implies there is still a close relation between P_2 and μ. The root mean square error in the case of fitting coefficients P_1, P_2 and P_3 in terms of μ are 2.0, 0.3 and 2.2, respectively. Surface UV radiation can thus be parameterized as a function of $\tau_{500\,\mathrm{nm}}$ and μ as follows

$$\mathrm{UV}=(32.1-3.7\times\mu)\times e^{(-2.5+1.8\times\mu)\times\tau_{500\,\mathrm{nm}}}+23.8\times\mu^{1.5}. \quad (2)$$

Figure 5 shows a comparison of UV estimated by Eq. (2) against observations for the 25% of data reserved for validation. The model performance was evaluated using the methodology recommended by Willmott (1982). An array of complementary difference and summary univariate indices were computed that included the mean absolute error (MBE=$N^{-1}\sum|P_i-O_i|$), the root mean square error (RMSE=$\left[N^{-1}\sum(P_i-O_i)^2\right]^{\frac{1}{2}}$), their systematic and unsystematic proportions or magnitudes (RMSE$_s$=$\left[N^{-1}\sum(\hat{P}_i-O_i)^2\right]^{\frac{1}{2}}$ and RMSE$_u$=$\left[N^{-1}\sum(P_i-\hat{P}_i)^2\right]^{\frac{1}{2}}$) and the average relative error represented by the index of agreement (AI=1−$\left[\sum(P_i-O_i)^2/\sum(|P_i'|+|O_i'|)^2\right]$), where O and P represent observation and prediction of UV, respectively. N is the number of cases. The parameters with a prime symbol are defined as $P_i'=P_i-\bar{O}$ and $O_i'=O_i-\bar{O}$. The parameter with a caret symbol is defined as $\hat{P}_i=a+bO_i$, where a and b are the intercept and slope of the least-squares regression between observations and predications of UV, respectively. The comparison between the estimations and observations of UV radiation showed that the MAE was ∼0.45 W m^{-2} and the RMSE was ∼0.63 W m^{-2}. The index of agreement is close to unit and the systematic difference contributes little to the mean square error (see Fig. 5). These suggested that the empirical formulation performed very well and can be used to estimate instantaneous UV with high accuracy if aerosol optical depth is available.

Using the above equations, aerosol radiative effect at the surface in the ultraviolet radiation band can be quantified. We calculated the ratio of UV radiation for $\tau_{500\,\mathrm{nm}}$ changing from 0.2 to 1.5 to that under a background condition (defined as $\tau_{500\,\mathrm{nm}}$=0.1), i.e. $\frac{\mathrm{UV}(\tau_{500\,\mathrm{nm}},\mu)}{\mathrm{UV}(\tau_{500\,\mathrm{nm}}=0.1\,\mu)}\times100$. Depending on θ, the ratio varies from 20% to 90% when $\tau_{500\,\mathrm{nm}}$ changes from 0.2 to 1.5. Taking the annual mean $\tau_{500\,\mathrm{nm}}$ (0.82) measured in Xianghe (Li et al., 2007b), the reductions in surface UV radiation induced by aerosols were from 24% to 74% when θ changed from 20° to 80° (see Fig. 6). It was revealed from ground-based and satellite data that a thick layer of haze often covered northern China primarily due to anthropogenic emissions (Li et al., 2007b; Xia et al., 2006); one would thus expect a significant impact on surface UV radiation by heavy aerosol loading, not only at this suburban site, but also in whole northern China. More importantly, rapid economic growth and population expansion over the past thirty years has led to a significant increase in aerosol loading over much

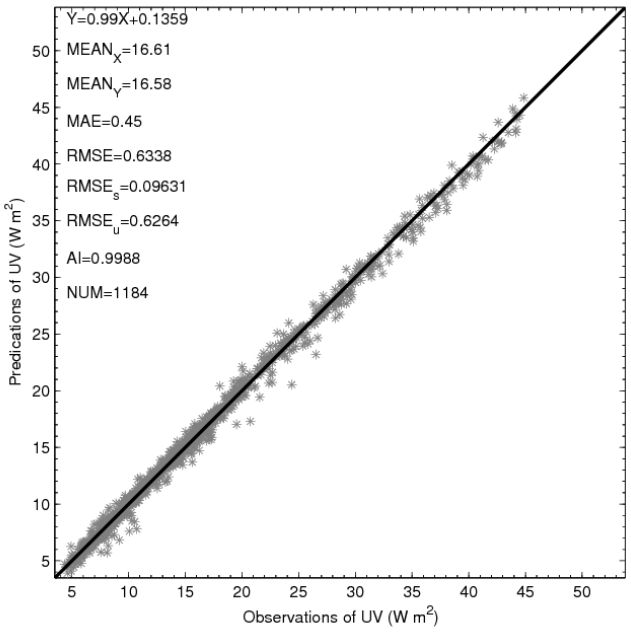

Fig. 5. Scatterplot of UV radiation between observation and model estimation. The black line represents the 1:1 relationship; also included are an array of complementary difference and univariate indices. The results were obtained using 25% of data reserved for validation.

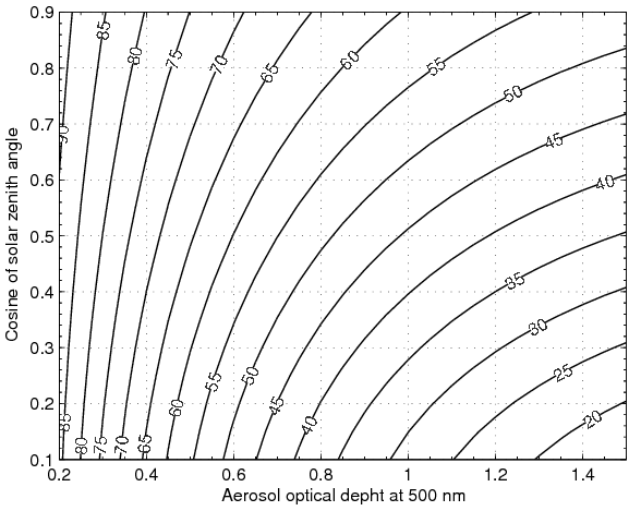

Fig. 6. The ratio of UV radiation with aerosol optical depth at 500 nm changing from 0.2 to 1.5 to that under background condition with aerosol optical depth at 500 nm equal to 0.1, i.e. $\frac{\mathrm{UV}(\tau_{500\,\mathrm{nm}},\mu)}{\mathrm{UV}(\tau_{500\,\mathrm{nm}}=0.1,\mu)} \times 100$.

of China (Luo et al., 2001; Xia et al., 2007b). It is a major cause for significant reductions in surface SW and UV radiation over much of China (Bai et al., 2003; Liang and Xia, 2005).

5 An all-weather model of UV radiation

Extension of Eq. (2) to data from other locations is restrictive, given that measurements of τ are very limited in terms of geography. More importantly, the equation is valid only for clear-sky conditions. Therefore, the clearness index (*Kt*) is introduced for estimating UV radiation for developing an all-weather model. Unlike τ that is only available at a very limited location, *Kt* is more objective and relatively more frequently available along with UV measurements. Furthermore, *Kt* denotes attenuation due to all scattering and absorption processes throughout the atmosphere.

To develop an empirical model, the whole 1-h data set under all-weather conditions was divided into two groups. The first one, comprising 75% of the total selected randomly, was used for the model development, while the remainder was used for validation. Figure 7 presents the values of UV against μ. *Kt* values are indicated by different colors. For a specified narrow range of *Kt*, UV increases with μ and the relationship is fit by the power law equation.

$$\mathrm{UV} = \mathrm{UV}_0 \times \mu^b, \quad (3)$$

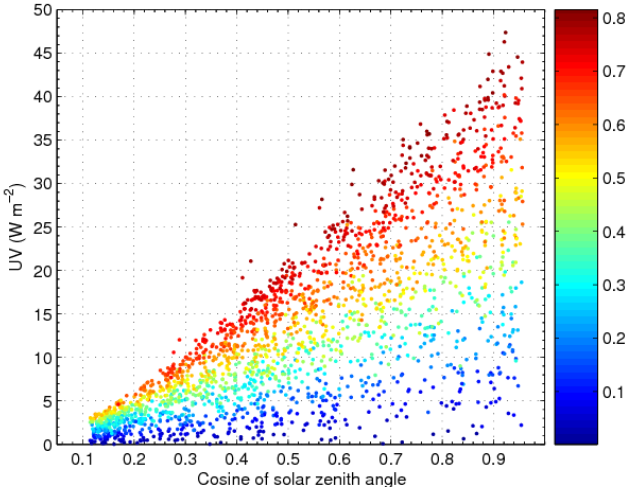

Fig. 7. UV radiation versus the cosine of the solar zenith angle. Data points for different clearness index (*Kt*) are represented by different colors. The values of UV for narrow ranges of the clearness index increase with the cosine of the solar zenith angle.

where UV_0 indicates the UV for one unit of μ and b determines how UV varies with μ. Considering the latitude of Xianghe, it is not possible to obtain direct measurements of UV_0 that requires zero solar zenith angles. The derivations of UV_0 are as follows. Based on UV measurements and associated μ, we can have hundreds of pairs of μ and UV for a specified narrow range of *Kt*. UV increases with μ and the relationship is fit by the power law equation (Eq. 3). UV_0 and b are derived simultaneously from the least-squares fitting of data points. UV_0 is then fitted as a function of *Kt* as follows

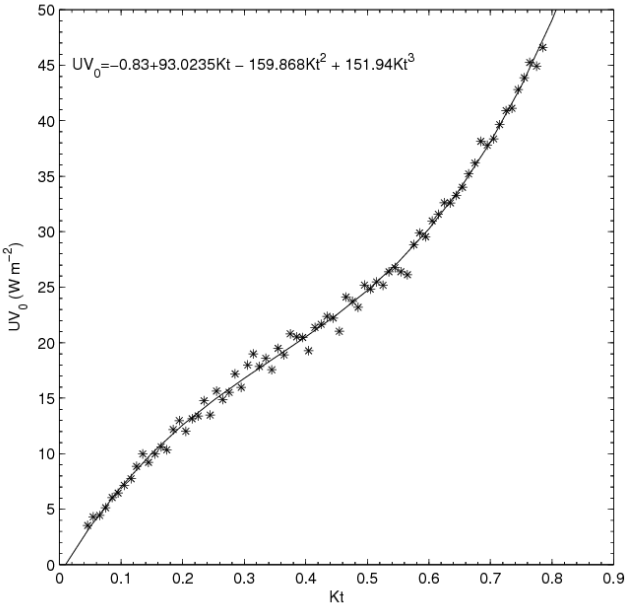

Fig. 8. Parameter UV_0 versus the clearness index (Kt) fitted with a cubic polynomial equation.

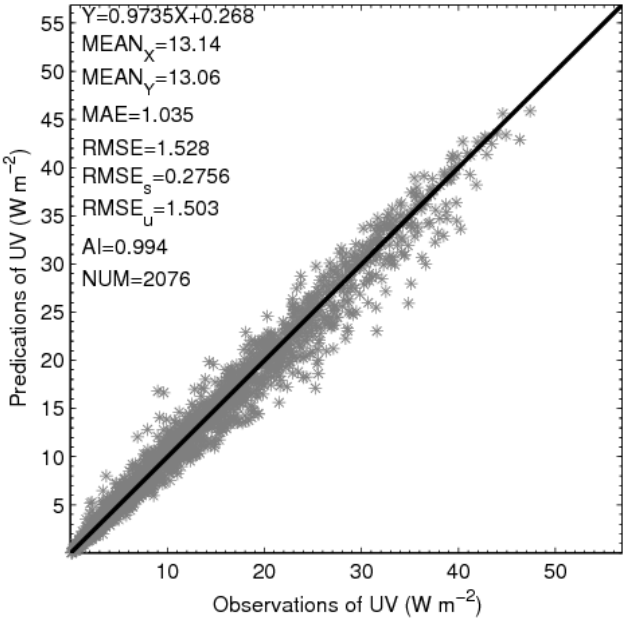

Fig. 9. Comparison between observed and estimated UV radiation under all-weather conditions. The black line represents the 1:1 relationship. Also marked is an array of complementary differences and univariate indices. The results were obtained using the 25% of data reserved for validation.

$$UV_0 = -0.83 + 93.0 \times Kt - 159.9 \times Kt^2 + 151.9 \times Kt^3. \quad (4)$$

The unit of the coefficients in Eq. (4) is $W\,m^{-2}$. Equation (4) can explain more than 95% of variance, and all relative root mean square errors are less than 10%. Figure 8 presents the scatter plot between UV_0 and Kt. The parameter b in Eq. (3) exhibited a moderately complex relation to Kt, but the variation of this parameter is very small and the standard deviation of b is 0.04. Thus, the mean value of this parameter ($\sim$1.06) is used and 95% of relative errors are less than 7%. Therefore, instantaneous UV is parameterized as follows

$$UV = (-0.83 + 93.0 \times Kt - 159.9 \times Kt^2 + 151.9 \times Kt^3) \times \mu^{1.06}. \quad (5)$$

A comparison of UV radiation estimated from Eq. (5) and observations is shown in Fig. 9. The MAE is $\sim$1.0 $W\,m^{-2}$ and the RMSE is $\sim$1.5 $W\,m^{-2}$. The index of agreement is close to unit and the systematic difference contributes little to the mean square error.

6 Conclusions

Two year's worth of surface radiation obtained at the Xianghe site in northern China were used to study the fraction of UV radiation to SW radiation. The monthly variation of this fraction and the dependence on τ and PWV were analyzed. Empirical models were developed to estimate surface UV radiation under clear-sky and all-weather conditions, respectively.

The annual mean F_{UV} was 3.85% and maximum monthly values occurred in summer and minimum appeared in winter. It follows from the regression equation that aerosols led to a reduction of about 0.0091 in F_{UV} per one unit increase in $\tau_{500\,nm}$ for PWV within 1.5$\sim$2.0 cm. A linear dependence of F_{UV} on PWV was derived for $\tau_{500\,nm}$ within 0.10$\sim$0.12, indicating an increase of 17% in F_{UV} for an increase of 1.0 cm in PWV. UV and SW radiation increased simultaneously but the former increased more, as a result, F_{UV} increased by 20% when the ground was covered with snow.

A simple and efficient clear-sky model was developed to estimate instantaneous surface UV radiation from $\tau_{500\,nm}$. Based on this parameterization, we inferred that surface UV radiation, depending on θ, was 90% to 20% of that under the background condition when $\tau_{500\,nm}$ changed from 0.2 to 1.5. Based on aerosol measurements at Xianghe, aerosol-induced reductions in surface UV was estimated to range from 24% to 74% for θ changing from 20° to 80°. The estimates of aerosol radiative effects on surface UV radiation are of significance to UV radiation estimations, air quality studies, as well as assessments of the impact of regional environmental change.

Surface UV radiation under all-weather conditions are linked with two independent quantities, i.e. μ and SW radiation. The first is easily calculated and the second is usually systematically measured in most radiometric stations. The dependences of UV radiation on these two quantities were parameterized and from which good estimations of UV can be obtained.

Acknowledgements. The research is supported by the Knowledge Innovation Project of Chinese Academy of Science (IAP07115), the Natural Science Foundation of China (40775009; 40575058), the National Basic Research of China (2006CB403706), and the NASA Radiation Science Program (NNG04GE79G) managed by Hal Maring.

Topical Editor F. D'Andrea thanks L. Alados-Arboledas and another referee for their help in evaluating this paper.

References

Alados, I., Mellado, J. A., Ramos, F., and Alados-Arboledas, L.: Estimating UV erythemal irradiance by means of neural networks, Photochem. Photobiology, 82(2), 351–358, 2004.

Alados, I., Gomera, M. A., Foyo-Moreno, I., and Alados-Arboledas, L.: Neural network for the estimate of UV erythemal irradiance using solar broadband irradiance, Int. J. Climatol., 27, 1791–1799, 2007.

Bai, J., Wang, G., and Hu, F.: The variation trends of ultraviolet radiation in clear sky during the last two decades in Beijing, Chinese J. Atmos. Sci., 2, 273–280, 2003.

Barbero, F. J., López, G., and Batlles, F. J.: Determination of daily solar ultraviolet radiation using statistical models and artificial neural networks, Ann. Geophys., 24, 2105–2114, 2006, http://www.ann-geophys.net/24/2105/2006/.

Boderker, G. E. and McKenzie, R. L.: An algorithm for inferring surface UV irradiance including cloud effects, J. Appl. Meteorol., 35, 1860–1877, 1996.

Calbó, J., Pages, D., and González, J. A.: Empirical studies of cloud effects on UV radiation: A review, Rev. Geophys., 43, RG2002, doi:10.1029/2004RG000155, 2005.

Cañada, J., Pedrós, G., and López, A.: Influence of the clearness index for the whole spectrum and of the relative optical air mass on UV solar irradiance for two locations in the Mediterranean area, Valencia and Cordoba, J. Geophys. Res., 4, 4759–4766, 2000.

Cañada, J., Pedrós, G., and Bosca, J. V.: Relationships between UV (0.290 – 0.385 μm) and broad band solar radiation hourly values in Valencia and Córdoba, Spain, Energy, 28, 199–217, 2003.

Ciren, P. and Li, Z.: Long-term global Earth surface ultraviolet radiation exposure derived from ISCCP and TOMS satellite measurements, Agric. For. Meteorol., 120, 51–68, 2003.

Diffey, B. L.: Solar ultraviolet radiation effects on biological systems, Phys. Med. Biol., 3, 299–328, 1991.

Foyo-Moreno, I., Vida, J., and Alados-Arboledas, L.: Ground based ultraviolet (290–385 nm and broadband solar radiation measurements in south-eastern Spain, Int. J. Climatol., 18, 1389–1400, 1998.

Foyo-Moreno, I., Vida, J., and Alaos-Arboledas, L.: A simple all weather model to estimate ultraviolet solar radiation (295–385 nm), J. Appl. Meteorol., 38, 1020–1026, 1999.

Foyo-Moreno, I., Alados, I., Olmo, F. J., and Alados-Arboledas, L.: The influence of cloudiness on UV global irradiance (295–380 nm), Agric. For. Meteorol., 120, 101–111, 2003.

Grimnes, A. A., Futsæther, C., Berre, B., et al.: Calibration of a UV broadband instrument – Eppley TUVR, 5th Workshop on Ultraviolet radiation measurements, Kassandra, Halkidiki, Greece, 2002.

He, Y., Zheng, Y., and He, D.: A summary of research on the effects of enhanced ultraviolet radiation on field ecosystems, Chinese J. Agrometeorol., 1, 47–52, 2002.

Kalashnikova, O. V., Mills, F. P., Eldering, A., and Anderson, D.: Application of satellite and ground-based data to investigate the UV radiative effects of Australian aerosols, Rem. Sens. Environ., 107, 65–80, 2007.

Koronakis, P. S., Sfantos, G. K., Paliatsos, A. G., Kaldellis, J. K., Farofalakis, J. E., and Koronaki, I. P.: Interrelations of UV-global/global/diffuse solar irradiance components and UV-global attenuation on air pollution episode days in Athens, Greece, Atmos. Environ., 19, 3173–3181, 2002.

Krzycin, J. W. and Puchalski, S.: Aerosol impact on the surface UV radiation from the ground-based measurements taken at Belsk, Poland, 1980–1996, J. Geophys. Res., 13, 16 175–16 181, 1998.

Liang, F. and Xia, X.: Long-term trends in solar radiation and the associated climatic factors over China for 1961–2000, Ann. Geophys., 23, 2425–2432, 2005, http://www.ann-geophys.net/23/2425/2005/.

Li, Z., Wang, P., and Cihlar, J.: A simple and efficient method for retrieving surface UV radiation dose rate from satellite, J. Geophys. Res., 4, 5027–5036, 2000.

Li, Z., Chen, H., Cribb, M., Dickerson, R., Holben, B., Li, C., Lu, D., Luo, Y., Maring, H., Shi, G., Tsay, S., Wang, P., Wang, Y., Xia, X., and Zhao, F.: Overview of east Asian studies of tropospheric aerosols, an international regional experiment (EAST-AIRE), J. Geophys. Res., 112, D22S00, doi:10.1029/2006/JD008853, 2007a.

Li, Z., Xia, X., Cribb, M., Mi, W., Holben, B., Wang, P., Chen, H., Tsay, S., Eck, T., Zhao, F., Dutton, E., and Dickerson, R.: Aerosol optical properties and its radiative effects in northern China, J. Geophys. Res., 112, D22S01, doi:10.1029/2006JD007382, 2007b.

Lü, D., Li,W., Li, F., Tang, Y., and Ma, H.: Observation and analysis of surface ultraviolet (UV-A, UV-B) spectral radiances in Changchun, Scientia Atmos. Sinica, 3, 343–351, 1996.

Ogunjobi, K. O. and Kim, Y. J.: Ultraviolet (0.280–0.400 μm) and broadband solar hourly radiation at Kwangju, South Korea: analysis of their correlation with aerosol optical depth and clearness index, Atmos. Res., 71, 193–214, 2004.

Papayannis, A., Balis, D., Bais, A., Van der Bergh, H., Calpini, C., Durieus, E., Fiorani, L., Jaquet, L., Ziomas I., and Zerefos, C. S.: Role of urban and suburban aerosols on solar UV radiation over Athens, Greece, Atmos. Environ., 32, 2193–2201, 1998.

Petteri, T., Amanatidis, G. T., and Heikkilä, A.: European Conference on atmospheric UV radiation: overview, J. Geophys. Res., 4, 4777–4785, 2000.

Renaud, A., Staehelin, J., Fröhlich, C., Philipona, R., and Heimo, A.: Influence of snow and clouds on erythemal UV radiation: analysis of Swiss measurements and comparison with models, J. Geophys. Res., 4, 4961–4969, 2000.

Schwander, H., Koepke, P., Kaifel, A., and Seckmeyer, G.: Modification of spectral UV irradiance by clouds, J. Geophys. Res., 107, 4296, doi:10.1029/2001JD001297, 2002.

Wang, P., Wu, B., and Zhang, W.: Analysis on the factors affecting surface UV radiation, Chinese J. Atmos. Sci., 1, 1–8, 1999.

Willmott, C. J.: Some comments on the evaluation of model performance, B. Am. Meteorol. Soc., 11, 1309–1313, 1982.

Xia, X., Xia, X., Chen, H., Wang, P., et al.: Variation of column-

integrated aerosol properties in a Chinese urban region, J. Geophys. Res., 111, D05204, doi:10.1029/2005JD006203, 2006.

Xia, X., Li, Z., Wang, P., Chen, H., and Cribb, M.: Estimation of aerosol effects on surface irradiance based on measurements and radiative transfer model simulations in northern China, J. Geophys. Res., 112, D22S10, doi:1.1029/2006JD008337, 2007a.

Xia, X., Chen, H., Goloub, P., Zhang, W., Chatenet, B., and Wang, P.: A compilation of aerosol optical properties and calculation of direct radiative forcing over an urban region in northern China, J. Geophys. Res., 112, D12203, doi:10.1029/2006JD008119, 2007b.

Zerefos, C. S. and Bais, A. F.: Solar ultraviolet radiation, modeling, measurements and effects, Springer Verlag, New York, 1997.